J Mater Sci: Mater Med (2008) 19:2993–3003
DOI 10.1007/s10856-008-3426-1

Controlled size and morphology of EDTMP-doped hydroxyapatite nanoparticles as model for ^{153}Samarium-EDTMP doping

YuLing Jamie Han · Say Chye Joachim Loo · Ngoc Thao Phung · Freddy Boey · Jan Ma

Received: 5 December 2007 / Accepted: 5 March 2008 / Published online: 25 March 2008

Abstract Hydroxyapatite (HA) nanoparticles have been studied as nano-sized carriers for the delivery of therapeutic agents. One important consideration for these carriers to be used effectively is their bio-distribution in vivo, of which particle size has a significant effect. In this work, HA nanoparticles doped with Ethylene-diamine-tetramethylene-phosphonate (EDTMP) were synthesized via co-precipitation as a model for HA doped with ^{153}Samarium (^{153}Sm) EDTMP. EDTMP has high affinity for radioactive ^{153}Sm isotopes that can emit both gamma and beta radiation. The effects of synthesis temperature, amount of dopant and hydrothermal treatment on the size of HA-EDTMP nanoparticles were therefore studied. The results showed that the EDTMP ligand was successfully incorporated in the nanoparticles without changing the crystal structure as shown from X-ray diffractometer (XRD) analysis. From the Field Emission Scanning Electron Microscopy (FESEM) and Transmission Electron Microscopy (TEM) micrographs, it was observed that shorter rod-like nanoparticles, obtained at low synthesis temperatures, became elongated needle-like nanoparticles with increasing temperature. Increasing dopant amount by five fold increases particle size slightly, while a two fold increase in dopant amount has no significant effect. Hydrothermal treatment increases particle crystallinity and results in smooth elongated rod-like structures. The size of HA nanoparticles doped with EDTMP can therefore be manipulated by controlling synthesis temperature and through hydrothermal treatment.

Y. J. Han · S. C. J. Loo (✉) · N. T. Phung · F. Boey · J. Ma
School of Materials Science and Engineering, Nanyang Technological University, Nanyang Avenue, Singapore 639798, Singapore
e-mail: joachimloo@ntu.edu.sg

1 Introduction

Hydroxyapatite ($Ca_{10}(PO_4)_6(OH)_2$, HA) is a major mineral component in animals and humans and is chemically similar to bone mineral [1, 2]. HA, in its different forms, is widely studied due to its excellent biocompatibility, bioactivity and similarity in chemical composition with human bone tissues [3–6]. As such, it is utilized in many biomedical applications such as orthopaedic implants [7–9], sustained drug release systems [10–15] and as an adsorbent in column chromatography for purification and separation of nucleic acids and proteins [16, 17]. A wide range of applications for HA is possible because its properties can be tailored by controlling its composition, for example by substitution in the crystal structure, particle size and morphology prior to usage [18–20].

HA has also been studied for the delivery of therapeutic agents. Matsumoto et al. [11] studied HA as a carrier of protein and modelled its release in vitro. Zhu et al. [21] showed adsorption of green fluorescence protein EGFP-N1 pDNA onto HA nanoparticle of size 40–60 nm. The results showed that HA nanoparticle EGFP-N1 pDNA conjugates transfected SGC-7901 cells in vitro and mice cells in vivo, and the pDNA were successfully expressed. These studies demonstrated the potential of HA nanoparticles to be used as a non-viral gene carrier or as a carrier of therapeutic agents.

There have been many studies of cancer treatment via radiation of ^{153}Samarium (^{153}Sm) isotopes and early phase I/II studies were published more than 10 years ago [22, 23]. It has since been developed to be used clinically for pain palliation in symptomatic bone metastases from several cancers, mainly prostatic and breast carcinoma [22–25]. Ethylene-diamine-tetramethylene-phosphonate (EDTMP) has a high affinity with ^{153}Sm [26] and so readily forms the complex—^{153}Sm-EDTMP (commercially known as

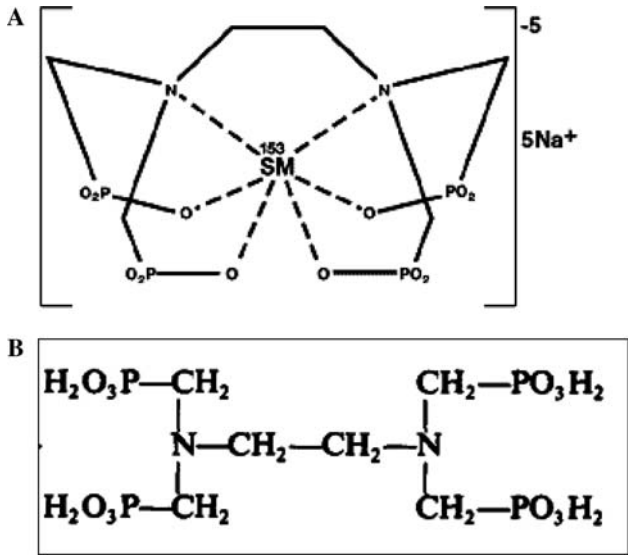

Fig. 1 (**a**) Structure of ^{153}Sm-EDTMP complex; (**b**) structure of EDTMP ligand

Quadramet®) such that $^{153}Sm^{3+}$ ion is in the centre of the ligand, as shown in Fig. 1. This structure is similar to what Mondry et al. [27] reported for Eu^{III}-EDTMP complex. Goeckeler et al. [28] were able to easily complexed ^{153}Sm with EDTMP in a single step, with more than 99% efficiency of ^{153}Sm-EDTMP. It was shown that this method of preparation is chemically stable and does not undergo any substantial decomposition for more than 48 h. Therapeutic and bioimaging applications of ^{153}Sm-EDTMP exploit the irradiation of short range (penetration depth of 2–3 mm) beta and gamma emissions for localised mortality of tumour cells. It reduces damage to bone marrow [29] and allows biodistribution and dosimetric assessment of the radiopharmaceutical in the individual patient [30].

Taking advantage of the fact that EDTMP has high affinity for ^{153}Sm and bone and/or HA, it provides a potential avenue to develop nano-sized HA conjugated with radioisotopes with EDTMP ligands for both therapeutic and bioimaging functions [31]. Hooi et al. [32] studied HA nanoparticles conjugated with radioisotopes ^{99m}Technetium (^{99m}Tc) for bioimaging. At the same time, they demonstrated a novel method to generate a drug-loaded or radiolabelled HA nanoparticles by exploiting the high-affinity (poly) phosphonate to HA interaction. Several studies had also been studied for therapeutic and in vivo imaging using HA-^{153}Sm-EDTMP particles. Chirby et al. [33] studied the adsorption of ^{153}Sm-EDTMP complex on the surface of HA particles and its skeletal uptake in rats. Clunie et al. [34] performed clinical trials on patients with chronic knee synovitis using HA-^{153}Sm-EDTMP particles as a carrier to obtain biodistribution data. Results were shown to be favourable and that HA-^{153}Sm-EDTMP particle is a potentially useful radiation synovectomy agent. O'Duffy et al. also used HA-^{153}Sm-EDTMP particle to [35] treat chronic synovitis and studied its long term effects of radiation exposure. The results showed that specific chromosomes-types abnormalities in peripheral lymphocytes are indictors of whole body radiation exposure, but it was found that there was no increased in scored chromosome types abnormalities after HA-^{153}Sm-EDTMP synovectomy.

Biodistribution data of HA-^{153}Sm-EDTMP particles intended for therapeutic treatments of specific cancerous sites is therefore important as initial studies. Maximizing the concentration of therapeutic nanoparticles at tumour sites is vital for greater treatment efficacy due to its short range beta emission. This minimizes damage to healthy cells in other parts of the body. Biodistribution is greatly affected by the uptake of macrophages of the mononuclear phagocyte system (MPS), of which one of the major determinants of clearance kinetics of these nanoparticles by the MPS macrophages is particle size [36, 37]. This study therefore aims to synthesize controlled sizes of HA nanoparticles doped with various amount of EDTMP as a model for HA-^{153}Sm-EDTMP nanoparticles. As $^{153}Sm^{3+}$ ion in the centre of the EDTMP ligand, doping HA nanoparticles with ^{153}Sm-EDTMP should not have significant difference in size in comparison to doping HA nanoparticles with EDTMP. In addition, by doping ^{153}Sm-EDTMP into HA, instead of surface tagging, would allow for further particle surface modification to enhance targeting and selective cellular uptake. In this paper, the effects of synthesis parameters (i.e. temperature, amount of EDTMP, hydrothermal treatment) on the size and morphology of HA-EDTMP nanoparticles is therefore reported.

2 Experimental

Calcium nitrate tetrahydrate ($Ca(NO_3)_2{\cdot}4H_2O$) from Riedel-deHaen, ammonium dihydrogen phosphate ($NH_4H_2PO_4$) from Aldrich, 25% v/v ammonium hydroxide (NH_4OH) from Honeywell, Multibone; Ethylene-diamine-tetramethylene-phosphonate ($NCH_2PO_3H_2$) from Izotop and Sodium hexametaphosphate (SHMP) from Sigma-Aldrich were purchased and used without further purification in this study. Hydroxyapatite (Sigma-Aldrich) [$Ca_{10}(PO_4)_6(OH)_2$] were used as reference for X-ray diffractometer (XRD) analysis.

Aqueous solutions of $Ca(NO_3)_2{\cdot}4H_2O$ (0.787 g in 13.2 ml water) and $NH_4H_2PO_4$ (0.23 g in 32 ml water) were prepared separately. 0.714 ml of water was added into 25 mg of EDTMP (per vial). EDTMP solution of 71 µl, 142 µl and 355 µl were added to the phosphate solution (these concentrations were chosen to provide substantial radioactivity for bioimaging purposes as previously tested). NH_4OH was added to the solutions to raise pH to 11 prior to the precipitation. $NH_4H_2PO_4$ was

added to the $Ca(NO_3)_2.4H_2O$ solution and stirred continuously for 3 h at different temperatures (0°C, 25°C, 65 °C and 85°C). The synthesized HA samples then undergo post-synthesis hydrothermal treatment, where 15 ml (5 mg/ml) of HA suspension was introduced into hydrothermal bombs (Parr acid digestion bombs, model 4744) and kept in a 200°C oven for 24 h. All samples were subsequently freeze dried (Alpha 1–4 LSC, Christ, Germany) to obtain the HA powders. Table 1 shows the labelling of the HA-EDTMP samples. Hydrothermal samples are identified with a suffix H. e.g. HA-0C-355H.

The morphology of the samples was characterized using Field Emission Scanning Electron Microscopy (FESEM), qualitative analysis of chemical bonds with Fourier Transform infrared spectrometry (FTIR). The crystal structure of the samples was examined using XRD while the particle sizes were measured using Dynamic Light Scattering (DLS) and Transmission Electron Microscopy (TEM).

2.1 X-ray diffractometer (XRD)

The phase structure of the coatings was identified using XRD (XRD-6000, Shimadzu, Tokyo, Japan) Parameters were set, using CuKα radiation, operating at 40 kV and 40 mA. Data were collected over a 2θ range from 20° to 50°, with a step size of 0.05° and dwell time of 10 s.

2.2 Fourier-transformed Infrared Spectroscopy (FTIR)

The molecular structure of doped HA was analyzed using FTIR (FTIR Spectrum GX, Perkin–Elmer, USA). The IR spectra of the powdered samples were recorded using a Perkin–Elmer 1600 FT-IR spectrometer. Samples were mixed with KBr (0.6 mg of sample to 140 mg KBr) in an agate mortar and pestle followed by compression into a pellet form. Sample spectra were collected over the range of 4,000–400 cm^{-1} at a resolution of 4 cm^{-1} and the reported data represents the average of 64 scans for a better signal to noise ratio.

2.3 Field emission scanning electron microscope (FESEM)

Morphology of powder samples was analyzed with FESEM (JSM 6340F, JOEL, Tokyo, Japan). Samples were prepared by scattering the powder samples onto carbon tape adhered to a platform, prior to coating with platinum. Micrographs were captured at vacuum condition with working distance of 8 mm, accelerating voltage of 5 kV and emission current of 12 μA.

2.4 Transmission electron microscope (TEM)

Particle size was characterized using the TEM (JEM 2010, JOEL, Tokyo, Japan). Samples were prepared by mixing a small quantity of sample in powder form in ethanol followed by ultra-sonication in a water bath. A carbon coated copper grid was used to collect the samples from the solution and the images were captured via an in-built camera.

2.5 Dynamic light scattering (DLS)

Dynamic light scattering (ZetaPlus, Brookhaven, USA) was used for hydrodynamic size measurements of the colloidal sample. A 0.1 wt% SHMP solution were first prepared. To SHMP solution 5 mg of nanoparticles were added, followed by dispersion via ultra-sonication to form a colloid. All measurements were performed at 25°C at a measurement angle of 90°.

3 Results

3.1 Fourier-transformed Infrared Spectroscopy (FTIR)

The FTIR spectra of HA doped and control samples synthesized at 85°C are shown in Figs. 2, 3 and 4. Control samples were synthesized under the same conditions but without EDTMP-doping. Since similar observations were made from the FTIR spectra of HA samples synthesized at different temperatures, only the FTIR spectra of HA-85C samples were shown. The spectra of the control samples exhibited all seven characteristic phosphate peaks of HA; triply degenerated asymmetric stretching mode of the P–O bond of at 1,100–1,000 cm^{-1}, non-degenerated symmetric stretching mode of the P–O bond at 990–920 cm^{-1}, triply degenerated bending mode of the P–O bond at 603 cm^{-1} and 566 cm^{-1}, and double degenerated bending mode of the O–P–O bond at 472 cm^{-1}. These results were in

Table 1 Labeling of HA-EDTMP samples synthesized with varying dopant amounts and temperatures

EDTMP amount (μl)	Temperature (°C)			
	0 °C	25 °C	65°C	85°C
71	HA-0C-71	HA-25C-71	HA-65C-71	HA-85C-71
142	HA-0C-142	HA-25C-142	HA- 65C-142	HA-85C-142
355	HA-0C-355	HA-25C-355	HA -65C-355	HA-85C-355

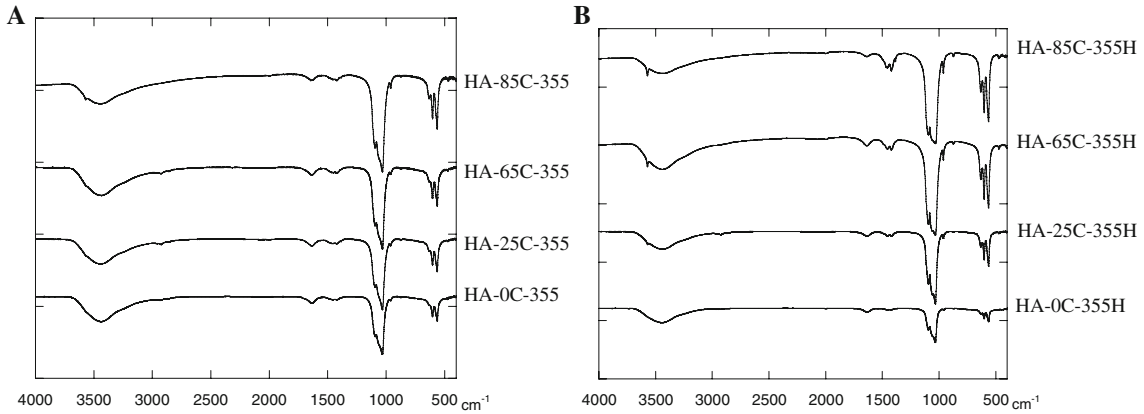

Fig. 2 FTIR spectra of HA-EDTMP samples prepared at 0°C, 25°C, 65°C and 85°C (**a**, before hydrothermal treatment; **b**, after hydrothermal at 200°C for 24 h.)

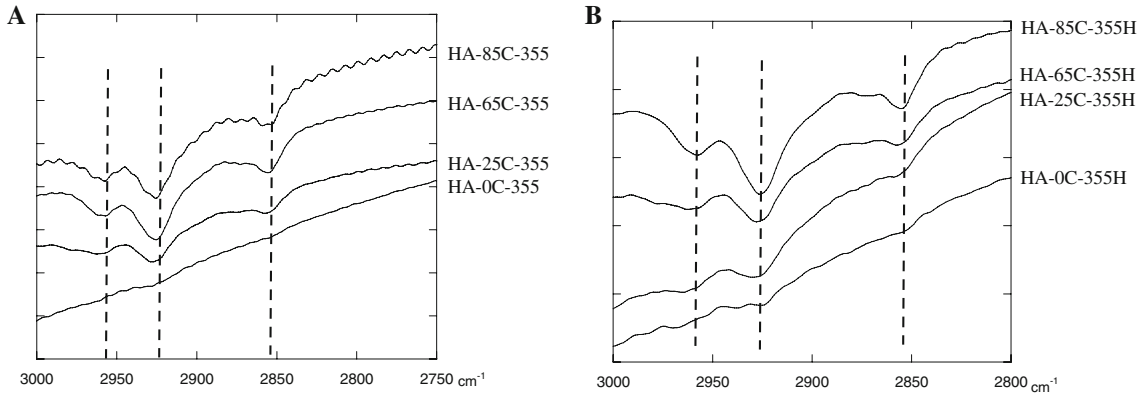

Fig. 3 FTIR spectra for the range of 3,000 cm^{-1} to 2,750 cm^{-1} and 2,800 cm^{-1} of HA-EDTMP samples prepared at 0°C, 25°C, 65°C and 85°C. (**a**, before hydrothermal treatment; **b**, after hydrothermal at 200°C for 24 h.)

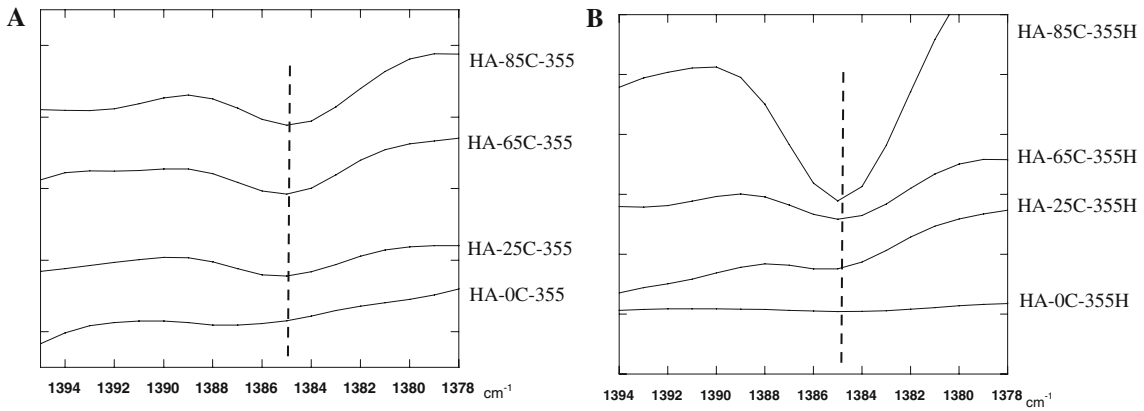

Fig. 4 FTIR spectra for the range of 1,394 cm^{-1} to 1,378 cm^{-1} of HA-EDTMP samples prepared at 0°C, 25°C, 65°C and 85°C. (**a**, before hydrothermal treatment; **b**, after hydrothermal at 200°C for 24 h.)

agreement to those reported by Koutsopoulos [38]. For the doped HA-EDTMP samples, additional peaks at 2,856 cm^{-1}, 2,925 cm^{-1} and 2,958 cm^{-1} corresponding to the $–CH_2–$ bonds and 1,384 cm^{-1} corresponding to ethylene diamine complex ($–N–CH_2–$) [39] were observed. The intensity of these peaks increased with increasing amount of EDTMP, from samples HA-85C-71 to HA-85C-355. These results show that EDTMP can be successfully doped into HA nanoparticles through a co-precipitation synthesis technique.

The carbonate (CO_3^{2-}) peaks at 1,421 cm^{-1}, 1,457 cm^{-1} and 873 cm^{-1} (Fig. 2) indicate B-type substitution, where CO_3^{2-} substitutes the phosphate positions in the HA lattice [40, 41]. It has been reported that the B-type substitution is predominant in HA synthesized from precipitation reactions [42–44]. The synthesis of HA and HA-EDTMP under atmospheric conditions allows for the dissolution of carbon dioxide from the atmosphere. Carbonate substitution increases at higher temperatures due to the formation of calcium carbonate during the heating of alkaline calcium nitrate solution prior to synthesis, thus the formation of carbonate-substituted HA [43]. After hydrothermal treatment, the phosphate stretching mode at 960 cm^{-1} increased in intensity, while there is a decrease in intensities for the carbonate peaks and hydroxyl vibration at 628 cm^{-1} and 3,564 cm^{-1} respectively. This decrease in intensity is due to the decomposition of carbonate into carbon dioxide at high temperature and pressure during hydrothermal treatment. Increased in peak intensity at 628 cm^{-1} and 3,564 cm^{-1} and PO_4^{3-} stretching mode at 960 cm^{-1}, also indicated an increased in particle crystallinity [44]. This increase in particle crystallinity is consistent with the XRD results which would be discussed later.

3.2 X-ray diffractometer (XRD)

Figures 5 and 6 plots the XRD diffraction patterns of HA and HA-EDTMP synthesized at various temperatures without and without hydrothermal treatment respectively. Since similar diffraction patterns were obtained for different amounts of doped EDTMP, only results from the 355 µl samples would be shown. The results show that the HA samples exhibited characteristic XRD diffraction patterns of HA [38]. No difference between the diffraction patterns of the control HA sample and HA-EDTMP was observed. This indicates that doping with EDTMP does not change the crystal structure of HA. Peak intensities were also observed to increase with synthesis temperature confirming that samples synthesized at higher temperatures (85°C) were indeed more crystalline, whereas samples synthesized at lower temperatures (0°C) were amorphous. This is supported by previous studies by Loo et al. [45] and Pang et al. [46]. Pang et al. concluded that particles synthesized at temperatures below 60°C resulted in particles with poor crystallinity, while crystallinity increased and crystallographic orientation improved above this transition temperature. Synthesis temperature is therefore a strong driving force for crystal growth, resulting in particles with higher crystallinity and higher aspect ratios.

After hydrothermal treatment, the crystallinity of HA nanoparticles drastically increased as reflected from the changes in peak intensities between Figs. 5 and 6. The fraction of crystalline phase (Xc) in the HA powders can be evaluated by the following equation according to Landi et al. [47]

$$Xc = 1 - V_{112/300}/I_{300} \quad (1)$$

where I_{300} is the intensity of (300) diffraction peak and $V_{112/300}$ is the intensity of the hollow between (112) and (300) diffraction peaks of HA. The calculated degrees of

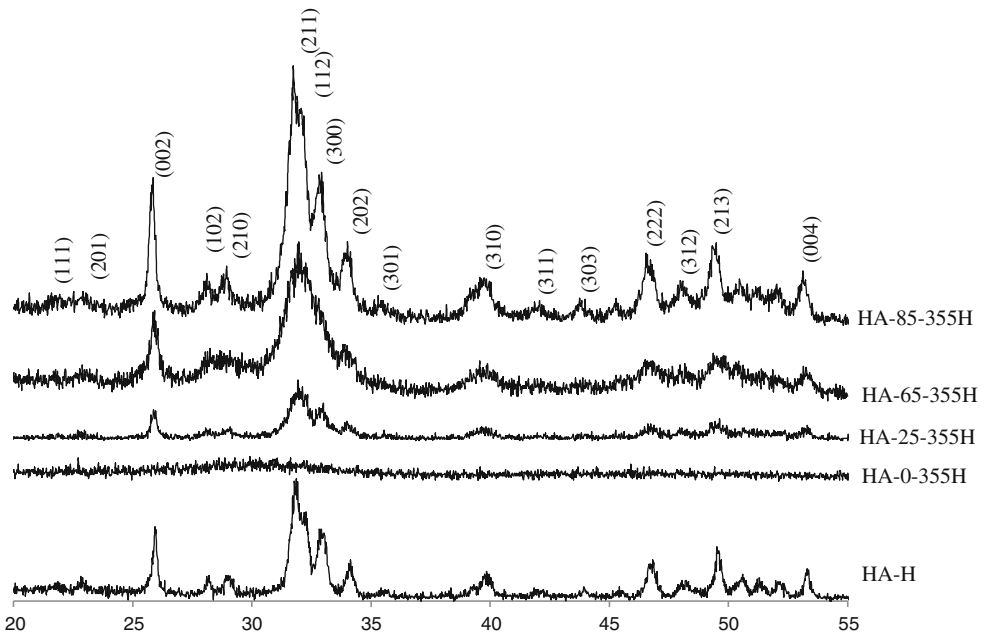

Fig. 5 XRD spectra of HA-EDTMP samples prepared at 0°C, 25°C, 65°C and 85°C doped with 355 µl of EDTMP, before hydrothermal treatment compared with commercial HA

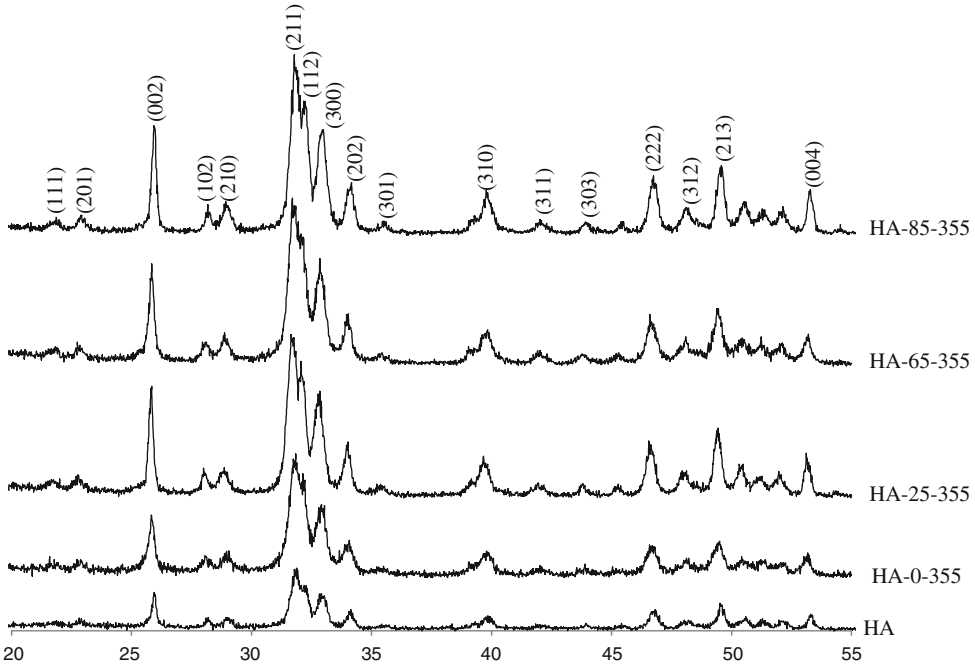

Fig. 6 XRD spectra of HA-EDTMP samples prepared at 0°C, 25°C, 65°C and 85°C doped with 355 µl of EDTMP,after hydrothermal treatment compared with commercial HA

Table 2 Degree of crystallinity for HA-EDTMP samples when doped with 355 µl, before and after hydrothermal treatment at 200°C for 24 h

Synthesis temperature (°C) for HA doped with 355 µl	Crystallinity Xc (%)	
	Before hydrothermal treatment	After hydrothermal treatment
0	Amorphous	0.555
25	0.103	0.566
65	0.120	0.564
85	0.363	0.658

crystallinity for these samples are summarized in Table 2. The crystallinity increased from amorphous to 0.363 by increasing the temperature from 0°C to 85°C. After hydrothermal, the Xc increased to 0.555 to 0.658 for 0°C to 85°C. These results verify that hydrothermal treatment indeed has a greater effect on crystallinity than synthesis temperature.

3.3 Field Emission Scanning Electron Microscope (FESEM) and Transmission Electron Microscope (TEM)

FESEM and TEM micrographs of HA nanoparticles doped with 355 µl EDTMP synthesized at different temperatures are shown in Fig. 7 and 8. Samples doped with 71 and 142 µl have similar size and shape, and hence are not shown here. From the micrographs, it is observed that HA nanoparticles were relatively uniform in shape and size. Particles synthesized at 0°C and 25°C were short rod-like with low aspect ratio, while those synthesized at higher temperatures (65°C and 85°C) were elongated with needle-like structure. Samples before hydrothermal treatment had particle surfaces that were uneven but these surfaces became more regular with smoother edges after hydrothermal treatment.

3.4 Dynamic light scattering (DLS)

Figure 9a and b plot the size of the nanoparticles synthesized at different temperatures with respect to EDTMP amount and after hydrothermal treatment. Two trends were observed; firstly, regardless of dopant amount, particles size increased with temperature and secondly, at a fixed temperature, increasing dopant amount increased particle size. The results obtained from the DLS were in good agreement with the measured sizes from the FESEM and TEM micrographs in Figs. 7 and 8. Also, there was a slight increase in particle size after hydrothermal treatment, with respect to the non-hydrothermal samples.

4 Discussion

The FTIR and XRD results showed that the present method of synthesis is a viable route to obtain HA-EDTMP

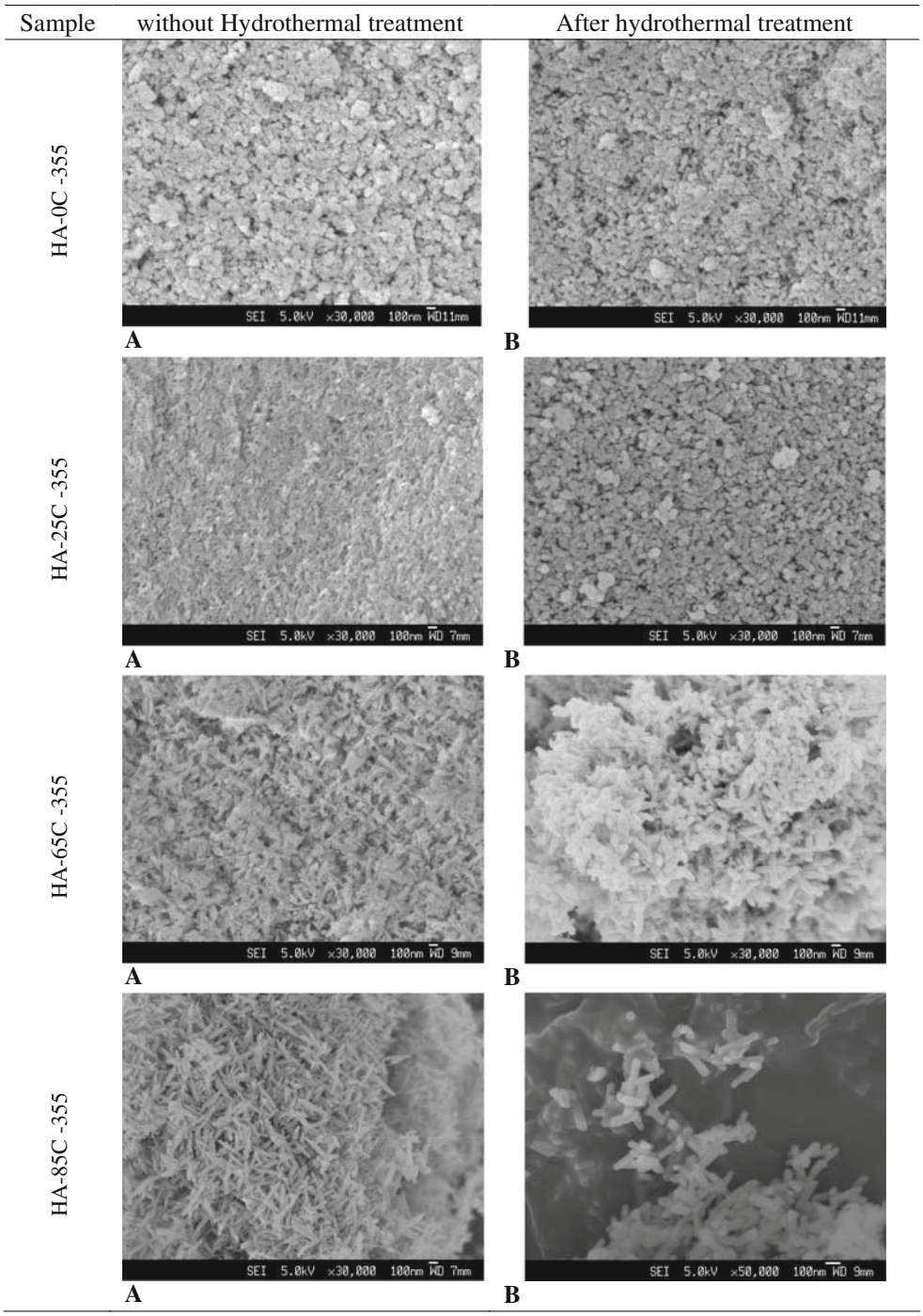

Fig. 7 FESEM micrograph of HA-EDTMP samples doped with 355 µl, synthesized at at 0°C, 25°C, 65°C and 85°C (**a**, before hydrothermal treatment; **b**, after hydrothermal at 200°C for 24 h.)

nanoparticles, while maintaining the crystal structure of HA. This is possible because the apatite structure can incorporate a wide variety of ions without changing its crystal structure. In another study by Vallet-Regı' et al silicate ions were similarly doped into HA nanoparticles via co-precipitation method [48]. It was reported that the substitution of $Si0_4^{4-}$ replaces the PO_4^{3-} groups with formation of vacancies at OH^- site so as to maintain the charge balance. The HA-EDTMP results therefore suggest that commercially available ^{153}Sm-EDTMP complex would very likely to be encapsulated into the HA nanoparticle, without much difference in particle size as the $^{153}Sm^{3+}$ ion is at the centre of the EDTMP ligand. The structures of EDTMP and its complex ^{153}Sm-EDTMP are shown in Fig. 1. $^{153}Sm^{3+}$ ion is surrounded by two nitrogen and four oxygen atoms in such a way that only one oxygen atom from each phosphonate group is coordinated to the central ion, similar to what Mondry et al. [27] has reported

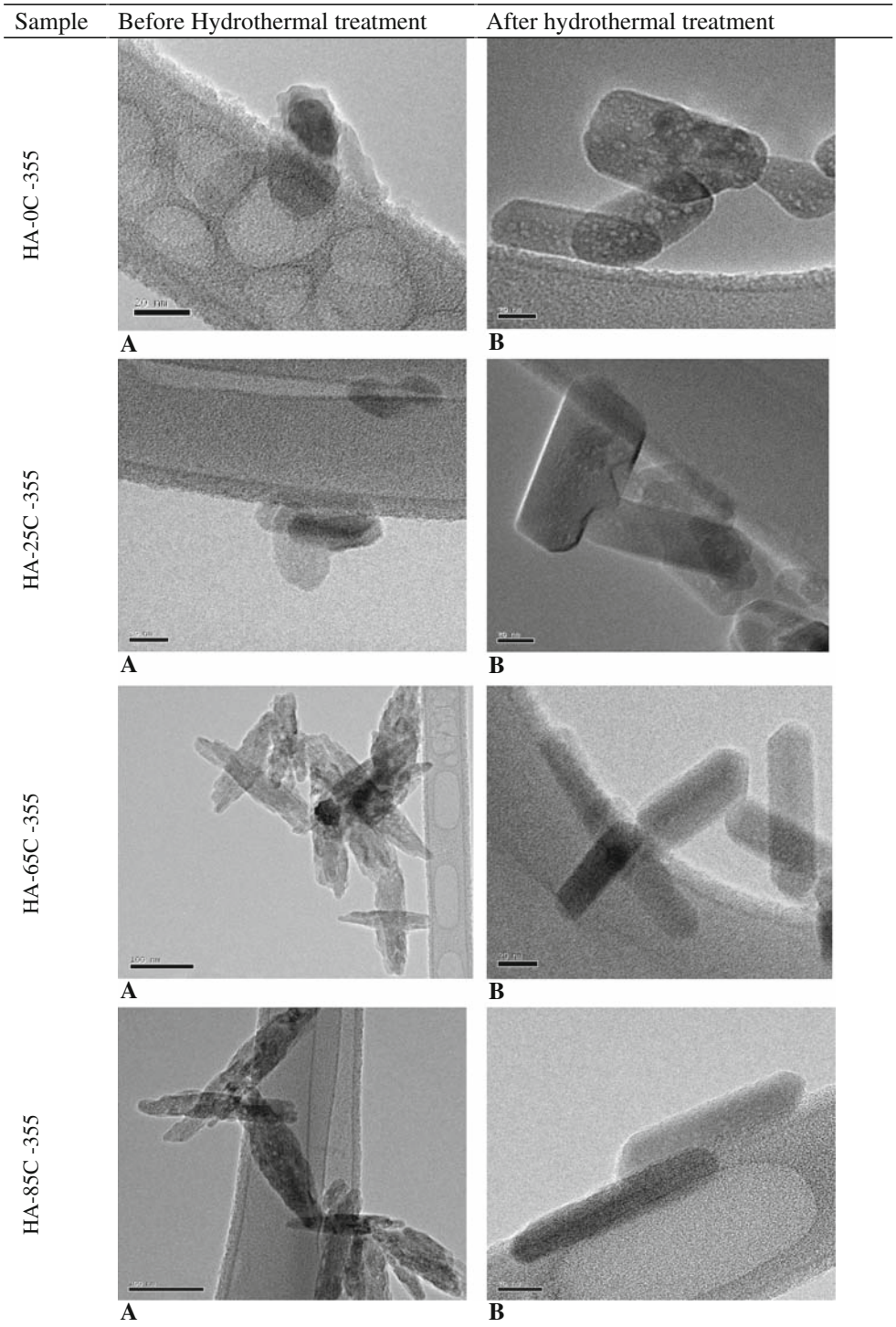

Fig. 8 TEM micrograph of HA-EDTMP samples doped with 355 µl, synthesized at at 0°C, 25°C, 65°C and 85°C (**a**, before hydrothermal treatment; **b**, after hydrothermal at 200°C for 24 h.)

on Eu^{III}-EDTMP complex. Hence, HA-EDTMP nanoparticles synthesised and characterised would act as a feasible model for studies on HA-^{153}Sm-EDTMP.

The morphology of HA-EDTMP nanoparticles changed from spherical to needle-like with increasing temperature as seen in FESEM and TEM micrographs in Figs. 7 and 8. DLS results also show the increment in size with temperature regardless of dopant amount. This is consistent with studies by Asaoka et al. and Gomez-Morales et al. [49, 50]. The precipitation and morphology trend can be explained through a crystal nucleation and growth mechanism. Kumar et al. studied precipitation of HA from different chemical reagents, stated that for HA precipitated from the salts of calcium and phosphate, an increase in temperature would increase the driving force for growth. Hence, it increases the aspect ratio from a spherical to needle-like

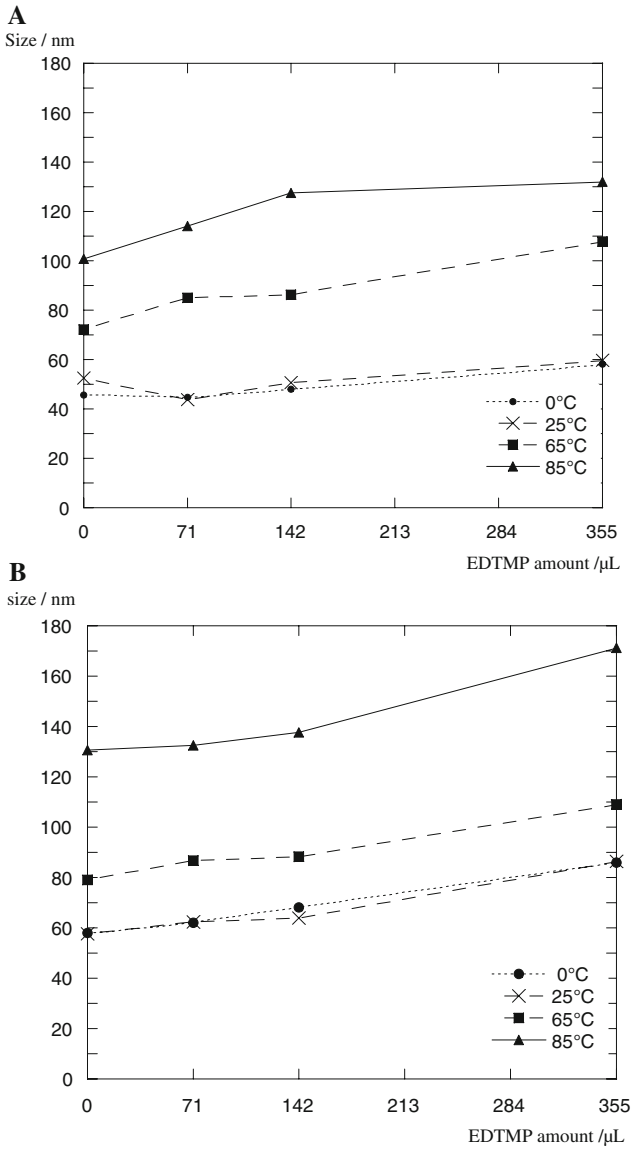

Fig. 9 Graph showing different sizes of HA sample and HA doped with 71, 142, 355 µl EDTMP, synthesized at 0°C, 25°C, 65°C and 85°C. (**a**, before hydrothermal; **b**, after hydrothermal treatment)

morphology [51]. Growth of particles occurs along the *c*-axis to develop into a needle-like structure, as the longer dimension of the crystals is oriented along the *c*-axis [52].

In general, chemical precipitation often undergoes high reaction-induced super-saturation, leading to high nucleation rates. According to Pang et al., a crystal nucleus usually has a rough surface due to the rapid production of insoluble materials [46]. This provides energetically favourable conditions for crystal growth as molecules adding on the nucleus have greater probability of attaching to it. At 65°C and 85°C, HA-EDTMP particles formed at higher rates, with respect to 0°C and 25°C, accounts for their rough surface as seen from the TEM micrographs.

Hydrothermal treatment results in particles with regular contours and uniform morphology and size. During hydrothermal treatment, the high temperature of 200°C and pressure cause recrystallization of the nanoparticles. The suggested phenomenon that occurs here is Ostwald ripening which is thermodynamically driven. Larger particles have lower energy state hence energetically favourable as compared to a smaller particle. In attempt to lower its overall energy, the particles seek to reduce surface area. Hence on the rough surface, molecules undergo diffusion to form regular contour to minimise surface area so as to be energetically stable. In addition, smaller particles tend to diffuse through solution and add to the surface of larger particle [52]. Consequently, the smaller particles continue to shrink, while larger particles continue to grow, resulting in particles with an increase in size and morphology with regular contours.

DLS results show that HA-EDTMP particle size increased with increasing dopant concentration for a constant synthesis temperature. The significant increase observed for particles doped with 355 µl of EDTMP corresponds to a five times increase with respect to 71 µl. The increase in aspect ratio is from the elongation along the *c*-axis to form needle-like structures [53]. Though the mechanism of doping is unclear at the moment, it is clear that EDTMP encapsulated in HA structure does not affect the crystal structure, as seen from the XRD results.

From the results, it is therefore conclusive that controlled sizes of HA-EDTMP with smoother surface contours and morphology can be achieved through a co-precipitation and hydrothermal synthesis technique. The synthesis temperature and hydrothermal treatment plays a vital role in the particle size and morphology.

5 Conclusion

HA nanoparticles doped with EDTMP were successfully synthesized through a co-precipitation technique as shown from FTIR results. XRD analysis shows that increasing synthesis temperature increased crystallinity. Subsequently, HA-EDTMP samples undergo a hydrothermal treatment to obtain particles with smoother surface morphology due to recrystallization. The hydrothermal treatment also increased the degree of crystallinity of the nanoparticles. DLS analysis also shows that particle size increased with an increase with synthesis temperature and dopant amount. Since it is not feasible to handle radioactive materials at our present facilities, this study of controlled size and morphology of HA-EDTMP could be use as a model for HA-^{153}Sm-EDTMP nanoparticles, since the $^{153}Sm^{3+}$ ion is sited in the centre of the ^{153}Sm-EDTMP complex. We believe the results obtained will be a good representation of that for HA-^{153}Sm-EDTMP nanoparticle synthesis.

Reference

1. K. Shigeru, T. Oku, S. Takagi, Hydraulic property of hydroxyapatite thermal decomposition product and its application as biomaterial. J. Ceram. Soc. **97**, 96–101 (1989)
2. M. Jarcho, C.H. Bolen, M.B. Thomas, J.J. Bobich, J.F. Kay, J. Doremus, Hydroxylapatite synthesis and characterization in dense polycrystalline form. J. Mater. Sci. **11**, 2027–2035 (1976)
3. M. Vallet-Regi, Ceramics for medical applications. J. Chem. Soc. **2**, 97–108 (2001)
4. L. Hermansson, L. Kraft, H. Engqvist, Chemically bonded ceramics as biomaterials. Key Eng. Mater. **247**, 437–442 (2003)
5. T. Kokubo, H.M. Kim, M. Kawashita, Novel bioactive materials with different mechanical properties. Biomaterials **24**, 2161–2175 (2003)
6. M. Shirkhanzadeh, Microneedles coated with porous calcium phosphate ceramics: effective vehicles for transdermal delivery of solid trehalose. J. Mater. Sci.—Mater. Med. **16**, 37–45 (2005)
7. D.A. Wahl, J.T. Czernuszka, D.A. Wahl, J.T. Czernuszka, Collagen-hydroxyapatite composites for hard tissue repair. Euro. Cell. Mater. **11**, 43–56 (2006)
8. J. Dumbleton, M.T. Manley, Hydroxyapatite-coated prostheses in total hip and knee arthroplasty. J. Bone Joint Surg. **86A**, 2526–2540 (2004)
9. J.S. Grimes, T.J. Bocklage, J.D. Pitcher, Collagen and biphasic calcium phosphate bone graft in large osseous defects. Orthopedics **29**, 145–148 (2006)
10. W. Paul, C.P. Sharma, Ceramic drug delivery: a perspective. J. Biomater. Appl. **17**, 253–264 (2003)
11. T. Matsumoto, M. Okazaki, M. Inoue, S. Yamaguchi, T. Toyonaga, Y. Hamada, J. Takahashi, Hydroxyapatite particles as a controlled release carrier of protein. Biomaterials. **25**, 3807–3812 (2004)
12. A. Uchida, Y. Shinto, N. Araki, K. Ono, Slow release of anticancer drugs from porous caclium hydroxyapatite ceramic. J. Orthopaed. Res. **10**, 440–445 (1992)
13. Y. Shinto, A. Uchida, F. Korkusuz, N. Araki, K. Ono, Calcium hydroxyapatite ceramic used as a delivery system for antibiotics. J. Bone Joint Surg. **74**, 600–604 (1992)
14. M. Itokazu, W. Yang, T. Aoki, A. Ohara, N. Kato, Synthesis of antibiotic-loaded interporous hydroxyapatite blocks by vacuum method and in vitro drug release testing. Biomaterials **19**, 817–819 (1998)
15. A. Barroug, M.J. Glimcher, Hydroxyapatite crystals as a local delivery system for cisplatin: adsorption and release of cisplatin in vitro. J. Orthopaed. Res. **20**, 274–280 (2002)
16. M.J. Gorbunoff, Protein chromatography on hydroxyapatite columns. Method. Enzymol. **117**, 370–380 (1985)
17. S. Doonan, Chromatography on hydroxyapatite. Methods Mol. B. **244**, 191–194 (2004)
18. L.L. Hench, Bioceramics: from concept to clinic. J. Amer. Ceram. Soc. **74**, 1487–1510 (1991)
19. W. Suchanek, M. Yoshimura, Processing and properties of hydroxyapatite-based biomaterials for use as hard tissue replacement implants. J. Biomed. Mater. Res. **13**, 94–117 (1998)
20. R.Z. LeGeros, Calcium phosphates in oral biology and medicine. Monogr Oral. Sci. **15**, 1–201 (1991)
21. S.H. Zhu, B.Y. Huang, K.C. Zhou, S.P. Huang, F. Liu, Y.M. Li, Z.G. Xue, Z.G. Long, Hydroxyapatite nanoparticles as a novel gene carrier. J. Nanoparticle. Res. **6**, 307–311 (2004)
22. J.H. Turner, P.G. Claringbold, E.L. Hetherington, P. Sorby, A.A. Martindale, A phase I study of samarium-153 ethylenediaminetetramethylene phosphonate therapy for disseminated skeletal metastases. J Clin. Oncol. **7**, 1926–1931 (1989)
23. J.H. Turner, P.G. Claringbold, A phase II study of treatment of painful multifocal skeletal metastases with single and repeated dose of samarium-153 ethylenediaminetetramethylene phosphonate. Euro. J. Cancer. **27**, 1084–1086 (1991)
24. J.F. Eary, C. Collins, M. Satbin, C. Vernon, S. Petersdorf, M. Baker, S. Hartnett, S. Ferency, S.J. Addison, F. Appelbaum, E.E. Gordon, Samarium-153-EDTMP biodistribution and dosimetry estimation. J. Nucl. Med. **34**, 1031–1036 (1993)
25. D.A. Podoloff, L.P. Kasi, E.E. Kim, F. Fossella, V.A. Bhadkamar, Evaluation of Sm-153-EDTMP as a bone imaging agent during a therapeutical trial. J. Nucl. Med. **32**, A918 (1991)
26. L.J. Peters, L. Milas, G.H. Fletcher, The role of radiation therapy in the curative treatment of metastatic disease. in *Cancer Invasion and Metastasis. Biologic and Therapeutic Aspects*, ed. by G.L. Nicolson, L. Milas (Raven Press, New York, 1984), pp. 411–420
27. A. Mondry, R. Janicki, From structural properties of the EuIII complex with ethylenediaminetetra (methylenephosphonic acid) (H8EDTMP) towards biomedical applications. Dalton Trans. **39**, 4702–4710 (2006)
28. W.F. Goeckeler, B. Edwards, W.A. Volkert, R.A. Holmes, J. Simon, D. Wilson, Skeletal localization of samarium-153 chelates: potential therapeutic bone agents. J. Nucl. Med. **28**, 495–504 (1987)
29. W.F. Goeckeler, D.E. Troutner, W.A. Volkert, B. Edwards, J. Simon, D. Wilson, ^{153}Sm radiotherapeutic bone agents. J. Radiat. Appl. Instum. B **13**, 479–482 (1986)
30. P.J. Cameron, P.F. Klemp, A.A. Martindale, J.H. Turner, Prospective ^{153}Sm-EDTMP therapy by whole body scintigraphy. Nucl. Med. Commun. **20**, 609–615 (1999)
31. E. Galiano, M. Stradiotto, A statistical analysis of the initial biodistribution of ^{153}Sm-EDTMP in a canine. Appl. Radiat. Isot. **63**, 79–85 (2005)
32. T.O. Hooi, J.S. Loo, F.Y. Boey, S.J. Russell, J. Ma, W.P. Kah, Exploiting the high-affinity phosphonate–hydroxyapatite nanoparticle interaction for delivery of radiation and drugs. J. Nanoparticle Res. **10**, 141–150 (2007)
33. D. Chirby, S. Franck, D.E. Troutner, Adsorption of samarium-153 complex with EDTMP on calcium hydroxyapatite. Appl. Radiat. Isot. **39**, 495–499 (1988)
34. G. Clunie, D. Liu, I. Cullum, J.C. Edwards, P.J. Ell, Samarium-153-particulate hydroxyapatite radiation synovectomy- Biodistribution data for chronic knee Synovitis. J. Nucl. Med. **36**(1), 51–57 (1995)
35. E.K. O'Duffy, F.J. Oliver, S.J. Chatters, H. Walker, D.C. Lloy, J.C. Edwards, P.J. Ell, Chromosomal analysis of peripheral lymphocytes of patients before and after radiation synovectomy with samarium-153 particulate hydroxyapatite. Rheumatology **38**(4), 316–320 (1999)
36. G. Storm, S.O. Belliot, T. Daemen, D.D. Lasic, Surface modification of nanoparticles to oppose uptake by the mononuclear phagocyte system. Adv. Drug Del. **17**, 31–48 (1995)
37. J. Brigger, C. Dubernet, P. Couvreur, Nanoparticles in cancer therapy and diagnosis. Adv. Drug Del. **54**, 631–651 (1995)
38. S. Koutsopoulos, Synthesis and characterization of hydroxyapatite crystals: A review study on the analytical methods. J. Biomed. Mater. Res. **62**, 600–612 (2002)
39. E. Princz, I. Szilágyi, K. Mogyorósi, I. Labádi, Lanthanide complexes of Ethylene Diamino Tetra Methylene Phosphonic Acid. J. Therm. Anal. Calorim. **69**, 427–439 (2002)
40. W.H. Emerson, E.E. Fisher, The infrared absorption spectra of carbonate in calcified tissues. Arch. Oral. Biol. **7**, 671–683 (1962)
41. V. Jokanović, D. Izvonar, M.D. Dramićanin, B. Jokanović, V. Živojinović, D. Marković, B. Dačić, Hydrothermal synthesis and nanostructure of carbonated calcium hydroxyapatite. J. Mater. Sci.—Mater. Med. **17**, 539–546 (2006)
42. D.G. Nelson, J.D. Featherstone, Preparation, analysis, and characterization of carbonated apatites. Calcif. Tissue Int. **34**, 569–581 (1982)

43. J. Barralet, S. Best, W. Bonfield, Carbonate substitution in precipitated hydroxyapatite: an investigation into the effects of reaction temperature and bicarbonate ion concentration. J. Biomed. Mater. Res. **41**, 79–86 (1998)
44. J. Barralet, J.C. Knowles, S. Best, W. Bonfield, Thermal decomposition of synthesised carbonate hydroxyapatite. J. Mater. Sci. Mater. Med. **13**, 529–533 (2002)
45. J.S.C. Loo, Y.W. Siew, S.H. Ho, Y.C. Boey, J. Ma, Synthesis and hydrothermal treatment of nanostructured hydroxyapatite of controllable sizes. J. Mater. Sci.—Mater. Med. **19**, 1389–1397 (2008)
46. Y.X. Pang, X. Bao, Influence of temperature, ripening time and calcination on the morphology and crystallinity of hydroxyapatite nanoparticles. J. Euro. Ceram. Soc. **23**, 1697–1704 (2003)
47. E. Landi, A. Tampieri, G. Celotti, S. Sprio, Densification behaviour and mechanisms of synthetic hydroxyapatites. J. Euro. Ceram. Soc. **20**, 2377–2387 (2000)
48. M. Vallet-Regı', D. Arcos, Silicon substituted hydroxyapatites. a method to upgrade calcium phosphate based implants. J. Mater. Chem. **15**, 1509–1516 (2005)
49. N. Asaoka, S. Best, J.C. Knowles, W. Bonfield, Characterisation of hydroxyapatites precipitated from different reacants. Bioceramics **8**, 331–337 (1995)
50. J. Gomez-Morales, J. Torrent-Burgues, T. Boix, J. Fraile, R. Rodriguez-Clemente, Investigations on the synthesis and crystallization of hydroxyapatite at low temperature. Cryst. Res. Tech. **36**, 15–26 (2001)
51. R. Kumar, K.H. Prakash, P. Cheang, K.A. Khor, Temperature driven morphological changes of chemically precipitated hydroxyapatite nanoparticles. Langmuir **20**, 5196–5200 (2004)
52. L. Ratke, P.W. Voorhees, *Growth and Coarsening: Ostwald Ripening in Material Processing*, 1st edn. (Springer, 2002), pp. 117–118
53. S.J. Zawacki, J.C. Heughebaert, G.H. Nancollas, The growth of nonstoichiometric apatite from aqueous solution at 37°C. II Effects of pH upon the precipitated phase. J. Colloid Interface Sci. **135**, 33–44 (1990)